Effect of substituents and anions on the phase behavior of Ru(II) sandwich complexes: exploring the boundaries between ionic liquids and ionic plastic crystals

Tominaga, Takumi
Ueda, Takahiro
Mochida, Tomoyuki

(Citation)
Physical Chemistry Chemical Physics,19(6):4352-4359

(Issue Date)
2017-02-14

(Resource Type)
journal article

(Version)
Accepted Manuscript

Effect of Substituents and Anions on the Phase Behavior of Ru(II) Sandwich Complexes: Exploring the Boundaries between Ionic Liquids and Ionic Plastic Crystals

Takumi Tominaga, Takahiro Ueda, Tomoyuki Mochida*

We recently developed ionic liquids containing cationic sandwich complexes. However, salts of the sandwich complexes often exhibit ionic plastic phases with high melting points. To explore the boundaries between ionic liquids and plastic crystals of sandwich salts, we investigated, in detail, the phase behavior of ruthenium complexes $[Ru(C_5H_5)(C_6H_5R)][X]$ ([**C0**][X]: R = H, [**C1**][X]: R = Me, [**C2**][X]: R = Et, [**C4**][X]: R = Bu). Among salts containing the anions PF_6^-, FSA^-, and $B(CN)_4^-$, [**C0**][X] and [**C1**][X] are solids that exhibit plastic phases at or above room temperature, whereas most of [**C2**][X] and [**C4**][X] are ionic liquids. Salts containing the $C(CN)_3^-$ anion exhibited lower melting points than the other salts. X-ray crystallography reveals that the cations and anions in most of these salts are arranged alternately in the solid state. However, in the case of [**C0**][$C(CN)_3$], the cations and anions are stacked independently, thereby providing weaker cation–anion interactions that account for the relatively low melting point of this salt.

Department of Chemistry, Graduate School of Science, Kobe University, Kobe, Hyogo 657-8501, Japan. E-mail: tmochida@platinum.kobe-u.ac.jp

†Electronic supplementary information (ESI) available: van der Waals volumes and radii of anions and cations (Tables S1, S2); phase transition data (Table S3); thermogravimetric traces (Fig. S1); DSC traces (Figs. S2–S4); polarizing microscopic images of [**C0**][FSA] and

[**C0**][$B(CN)_4$] (Figs. S5 and S6); temperature dependence of viscosities (Fig. S7); packing diagrams of [**C0**][FSA] and [**C0**][$B(CN)_4$] (Fig. S8); powder XRD patterns (Fig. S9); ORTEP drawings of the molecular structure (Fig. S10); cell parameters of [**C0**][FSA] and [**C0**][$B(CN)_4$] (Table S4). CCDC-1489227 ([**C0**][$C(CN)_3$]) and -1489228 ([**C2**][PF_6]) contain the supplementary crystallographic data. For ESI, see DOI: 10.1039/

INTRODUCTION

Ionic liquids have attracted significant attention over the past few decades, because of their negligible vapor pressures, non-flammability, high ionic conductivities, and other versatile solvent properties.[1] The majority of ionic liquids contain organic cations such as imidazolium, ammonium, or phosphonium, while fluorinated anions such as bis(trifluoromethanesulfonyl)amide (Tf_2N^-), bis(fluorosulfonyl)amide (FSA^-), or hexafluorophosphate (PF_6^-) are often used as counter anions. Recently, ionic liquids bearing either metal-containing anions or cations have attracted attention owing to the unique properties imparted by the metal ion. Several ionic liquids have metal-containing anions,[2] whereas fewer ionic liquids with metal-containing cations have been reported.[3]

We have developed various ionic liquids derived from cationic sandwich complexes that exhibit intriguing magnetic properties and chemical reactivities.[4] However, salts of sandwich complexes often exhibit plastic phases that have high melting points.[5] Therefore, a better understanding of these salts is important, as this will lead to the improved design of organometallic salts, with either ionic liquid or plastic crystal characteristics. Furthermore, ionic plastic phases, such as those exhibited by alkylammonium salts and other globular organic cations, have recently attracted attention owing to their high ionic conductivity.[6] Hence, we consider that the further exploration of organometallic ionic plastic crystals is important.

To investigate the boundaries between ionic liquids and plastic crystals of the salts of sandwich compounds, the phase behavior of [Ru(Cp)(C_6H_5R)][X] (Cp = cyclopentadienyl) was systematically investigated, the results of which are reported herein. Cationic ruthenium complexes were chosen because of their stability and ease of preparation.[7] For the systematic investigation, cations with and without alkyl substituents (R = H, Me, Et, and Bu) were used, along with the anions PF_6^-, FSA^-, $B(CN)_4^-$, and $C(CN)_3^-$ (Fig. 1). Among the anions, $B(CN)_4^-$ (V = 117 Å^3) is the largest, but it is still smaller than Tf_2N^- (V = 158 Å^3) (Table S1, ESI†). The use of anions having octahedral, bent, tetrahedral, and trigonal structures, will lead to an understanding of the effect of anion geometry on the properties of these materials. The van der Waals volumes of the cations are 187–260 Å^3 for alkyl groups (R) that range from H through to Bu (Table S2; ESI†), and the correlation between cation–anion radius ratios and phase behavior is also of interest. Among the salts represented in Fig. 1, the crystal structure and phase transition of [**C0**][PF_6] has been reported by Grepioni, with the salt exhibiting a phase transition to the plastic phase at 59.3 °C (ΔS_m = 12.5 J mol^{-1} K^{-1}).[8] The thermal properties of [**C4**][X] (X = PF_6^-, FSA^-) and the crystal structure of [**C4**][PF_6] have been reported in our previous paper.[7]

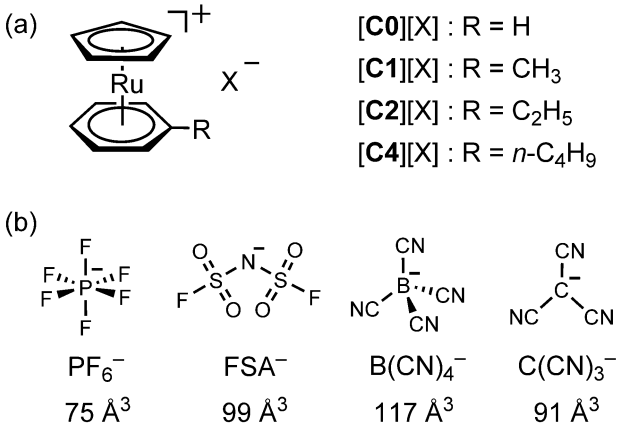

Fig. 1 (a) Structural formulas of the [Ru(Cp)(C_6H_5R)][X] complexes investigated herein. (b) Structural formulas of the anions (X^-). The van der Waals volume provided below each anion is estimated from density functional theory (DFT) calculations.

Results and Discussion

Synthesis and properties

The PF_6^- salts were synthesized either by the reported method,[8] or by the reaction of $[Ru(Cp)(NCCH_3)][PF_6]$ with the required arene ligand in acetonitrile.[9] The remaining salts were prepared from the corresponding PF_6^- salt by anion exchange. The products were either white solids or pale yellow liquids at room temperature. Most of [**C0**][X] and [**C1**][X] were solids, whereas most of [**C2**][X] and [**C4**][X] were liquids. The [**C1**][FSA] and [**C1**][$B(CN)_4$] solids were somewhat greasy, although the former solid was not a plastic crystal at room temperature (see below).

The decomposition temperatures (T_{dec}; −3 wt.%) of [**C4**][X], as determined by thermogravimetric (TG) analysis, are included in Table 1, while the corresponding TG curves are shown in Fig. S1 (ESI†). The salts with the anions PF_6^-, $B(CN)_4^-$, and FSA^- showed comparable thermal stability (T_{dec} = 228–265 °C), whereas the $C(CN)_3^-$ salt exhibited a much lower decomposition temperature (T_{dec} = 177 °C). The same tendency was observed for the decomposition of [**C0**][X] (Table 1), thereby confirming the lower thermal stability imparted by the anion $C(CN)_3^-$.

Thermal properties

The thermal properties of the salts were investigated via differential scanning calorimetry (DSC). The melting points and other relevant parameters are listed in Table 1. Their phase transition data and DSC traces are summarized in Table S3 and Figs. S2–S4 (ESI†). The phase sequences of the salts are shown in Fig. 2. As seen in this figure, with the exception of salts containing the anion $C(CN)_3^-$, [**C0**][X] and [**C1**][X] were solids up to high temperatures (Fig. 2a-b), whereas most of [**C2**][X] and [**C4**][X] were liquids at room temperature (Fig. 2c-

d). Therefore, the phase behavior was found to be strongly dependent on the substituent of the cation.

Most of [**C0**][X] and [**C1**][X] salts were solids up to high temperatures and exhibited plastic phases at or above room temperature, as indicated by the asterisks in Fig. 2a-b. These plastic phases were confirmed by polarizing microscope observations (Figs. S5 and S6, ESI†) and powder XRD experiments (see below). [**C0**][$C(CN)_3$] and [**C1**][$C(CN)_3$] were exceptional in that they exhibited liquid phases (T_m = 90.2 °C and T_m = −1.3 °C, respectively). Their melting entropies (ΔS_m) were 27.5 and 73.7 J mol^{-1} K^{-1}, respectively. These salts did not exhibit plastic phases, which is probably due to the planar anion, which is unable to rotate isotropically. These $C(CN)_3^-$ salts, as well as [**C1**][FSA] (T_m = 265 °C), exhibited melting points, whereas the remaining salts decomposed at high temperatures without melting.

In contrast, except for the PF_6^- salts, [**C2**][X] and [**C4**][X] exhibited liquid phases at room temperature. Most of these salts demonstrated glass transitions upon cooling from the liquid state (T_g = −87 to −69 °C). Both melting points and glass transition temperatures were observed for [**C1**][$C(CN)_3$] and [**C2**][$B(CN)_4$], for which T_g/T_m ratios were 0.684 and 0.682, respectively. These values are in agreement with the empirical rule for molecular liquids (T_g/T_m = 2/3).[10] [**C2**][PF_6] and [**C2**][$B(CN)_4$] showed plastic phases below their melting points. [**C2**][PF_6] (T_m = 161.3 °C, ΔS_m = 13.2 J mol^{-1} K^{-1}) showed a significantly higher melting point as compared with the corresponding Fe-containing complex [Fe(Cp)($C_6H_5C_2H_5$)][PF_6] (T_m = 111.9 °C, ΔS_m = 39.7 J mol^{-1} K^{-1}).[11] This tendency is likely to be ascribed to the presence of the plastic phase in [**C2**][PF_6], which stabilizes the solid phase at high temperatures. It is interesting to note that a slight change in the cation volume can cause such a significant change in the melting point.

As shown above, most of unsubstituted salts, or those having methyl substituents, are solids that exhibit plastic phases (except for the $C(CN)_3$ salts), whereas most of the salts bearing an

ethyl or longer substituent are ionic liquids. Thus, the boundary between plastic and ionic liquid behavior lies between methyl and ethyl substitution, indicating that the conformational freedom of the substituent is a crucial factor in determining thermal behavior. In the case of the imidazolium salts, it seems that Mmim (Mmim = 1,3-dimethylimidazolium cation) salts have no plastic phases, and elongation of the alkyl substituent (from methyl to ethyl) only serves to decrease their melting points.[6g] Plastic phases have been observed in 1,2-bis[*N*-(*N*′-alkylimidazolium)]ethane salts[6g] and imidazolium methanesulfonate.[12] Therefore, the phase transition characteristics of salts of sandwich complexes are notably different from those of imidazolium salts. Plastic phases occur owing to the quasispherical shape of the cation, and the introduction of an alkyl chain results in the loss of this plastic phase and the appearance of a liquid phase. Concerning the nature of the anion, $C(CN)_3^-$ salts exhibit notably lower melting points than the remaining salts. Therefore, the utilization of planar anions may be advantageous for decreasing the melting point of these materials. This tendency is likely to be related to their crystal structures as discussed below. As related salts, $[Fe(C_5Me_5)_2][C(CN)_3]$ and $[Fe(C_6Me_6)_2][C(CN)_3]_2$ are known,[13,14] but their thermal properties are unknown.

Table 1 Glass transition temperature (T_g), melting point (T_m), melting entropy (ΔS_m), melting enthalpy (ΔH_m), and decomposition temperature (T_{dec}) of the salts synthesized in this study.

	T_g (°C)	T_m (°C)	ΔS_m (J mol^{-1} K^{-1})	T_{dec} (°C)
[**C0**][PF_6]				360 [a]
[**C0**][FSA]				300 [a]
[**C0**][$B(CN)_4$]				280 [a]
[**C0**][$C(CN)_3$]		90.2	27.5	150 [a]
[**C1**][PF_6]				260 [a]
[**C1**][FSA]		265 [a]		–[d]
[**C1**][$B(CN)_4$]				210 [a]
[**C1**][$C(CN)_3$]	–87	–1.3	73.7 [b]	–[d]
[**C2**][PF_6]		161.3	13.2	–[d]
[**C2**][FSA]		16.9	64.6	–[d]

[**C2**][B(CN)$_4$]	–69	22.6	16.1	235 [e]
[**C2**][C(CN)$_3$]	–86			–[d]
[**C4**][PF$_6$] [c]		87.0	22.8	228 [e]
[**C4**][FSA] [c]	–82			265 [e]
[**C4**][B(CN)$_4$]	–69			229 [e]
[**C4**][C(CN)$_3$]	–77			177 [e]

[a]Visual observation. [b]Including the contribution of a solid phase transition near the melting point. [c]Data from Ref. 7. [d]Not measured. [e]Determined by TG analysis (−3 wt.%, 10 K min^{-1}).

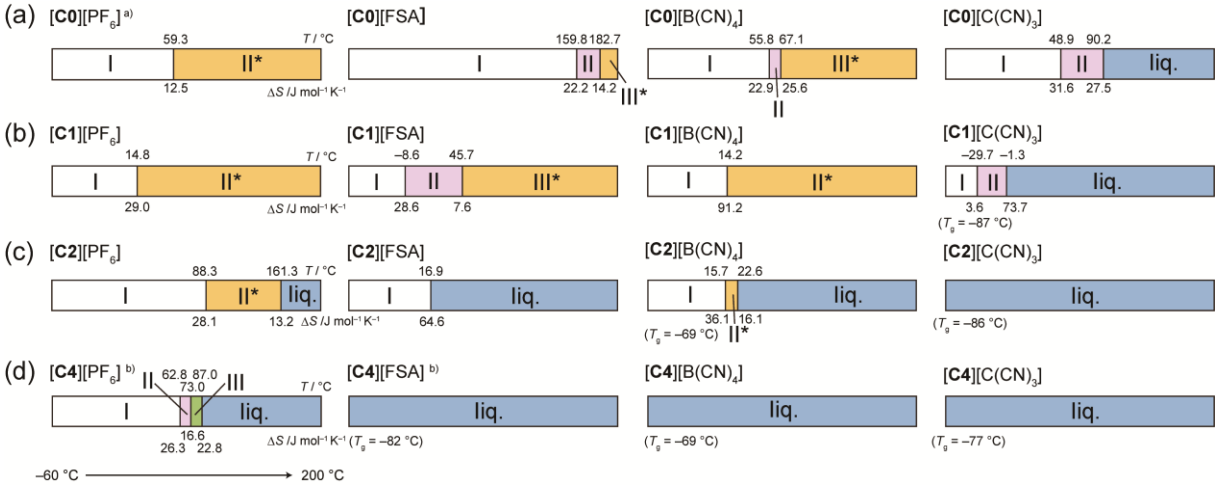

Fig. 2 Phase sequences of (a) [**C0**][X], (b) [**C1**][X], (c) [**C2**][X], and (d) [**C4**][X]. The transition temperatures (°C) and transition entropies (J K^{-1} mol^{-1}) are shown above and below each bar chart, respectively. Plastic phases are indicated by asterisks (*). [a]Ref. 8. [b]Ref. 7.

Viscosities of the ionic liquids

It is known that the anion B(CN)$_4^-$ tends to produce ionic liquids with low viscosities.[15] Therefore, we measured the temperature dependence of the viscosities of [**C2**][B(CN)$_4$] and [**C4**][B(CN)$_4$] (Fig. S7; ESI†). These two salts exhibited comparably low viscosities at room temperature, $\eta_{25\ °C}$ = 48.7 and 42.0 mPa s, respectively (Table 2). The viscosity of [**C4**][B(CN)$_4$] was found to be approximately half that of [**C4**][FSA] ($\eta_{25\ °C}$ = 90.8 mPa s).[7] This result is in contrast to the almost identical viscosities found for the analogous

imidazolium salts [Emim][B(CN)$_4$] ($\eta_{20\,°C}$ = 22 mPa s) and [Emim][FSA] ($\eta_{20\,°C}$ = 19 mPa s) (Emim = 1-ethyl-3-methylimidazolium cation).[16,17] These data suggest that B(CN)$_4^-$ is effective at lowering the viscosities of ionic liquids containing cationic sandwich complexes, which are usually highly viscous.

The temperature dependence of the viscosity was analyzed using the Vogel–Fulcher–Tammann (VFT) equation ($\eta = \eta_0 \exp[DT_0/(T–T_0)]$),[18] where T_0 is the ideal glass-transition temperature and D is a parameter that reflects the deviation from Arrhenius behavior and the fragility of the glass state (Table 2). The parameters obtained for the B(CN)$_4^-$ salts are very similar to those obtained for [Bmim][Tf$_2$N] (Bmim = 1-butyl-3-methylimidazolium cation).

Table 2 Viscosity data and relevant parameters for liquid samples.

	$\eta_{25\,°C}$ (mPa s)	D	η_0 (mPa s)	T_0 (°C)
[**C2**][B(CN)$_4$]	48.7	5.0	0.15	–112.8
[**C4**][B(CN)$_4$]	42.0	2.4	0.46	–78.0
[**C4**][FSA] [a]	90.8	6.5	0.21	–130.8
[**C4**][Tf$_2$N] [a]	136.6	5.6	0.22	–115.2
[Bmim][Tf$_2$N] [b]	49 [c]	4.7	0.25	–108.5

[a]Data from Ref. 7. [b]Data from Ref. 19. [c]Value at 20 °C.

Crystal structures

X-ray crystal structure studies reveal that [**C2**][PF$_6$], [**C0**][B(CN)$_4$], and [**C0**][FSA] have alternating anion–cation arrangements in their respective crystals, similar to [**C0**][PF$_6$][8] and [**C4**][PF$_6$].[7] In contrast, [**C0**][C(CN)$_3$] appears to form a segregated-stack structure.

The packing diagram of [**C2**][PF$_6$], determined at 100 K, is shown in Fig. 3. This salt crystallized in the $P2_12_12_1$ space group, with one crystallographically independent cation and anion. The cations and anions are alternately packed, with close contacts between the ring hydrogen atoms in the cation and the fluorine atoms in the anion (F$\cdots$H$_{benzene}$ = 2.50–2.61 Å, F$\cdots$H$_{Cp}$ = 2.42–2.66 Å); these separations are shorter by 0.10–0.25 Å than the sum of the

respective Van der Waals radii. [**C0**][$B(CN)_4$] and [**C0**][FSA] also exhibited structures in which the cations and anions are alternately packed (Fig. S8, ESI†), but we refrain from a detailed discussion of their structures owing to the disorder of the Cp and benzene rings. The structure of [**C0**][FSA] closely resembles that of [$Co(Cp)_2$][FSA].[20] The anions in these salts assume *trans* conformations in which they exhibit two-fold disorder. Unlike [$Co(Cp)_2$][FSA],[20] [**C0**][FSA] exhibited no phase transition accompanying the order–disorder of the anion, down to −150 °C.

According to the radius ratio rule in ionic crystals, coordination numbers are expected to be six for cation–anion radius ratios of 0.41–0.73, and eight for ratios greater than 0.73.[21] In the present salts, the number of nearest neighbor molecules (i.e., the number of nearest anions to a given cation, and vice versa) in [**C0**][X] (X = $B(CN)_4^-$, FSA^-, and PF_6^-) is eight, whereas the analogous number for [**C2**][PF_6] and [**C4**][PF_6] is six. Based on the van der Waals radii of these molecules (Tables S1 and S2, ESI†), the radius ratios (r_{anion}/r_{cation}) for the former salts are derived to be 0.74–0.86, whereas those for the latter salts are 0.66–0.70. Therefore, the cation–anion arrangements are in agreement with the radius ratio rule.

The packing diagrams of [**C0**][$C(CN)_3$], determined at 173 K, are shown in Fig. 4. This salt crystallized in the $P2_1/n$ space group, with two crystallographically independent cations and anions within the unit cell. The cation showed no disorder. In striking contrast to the other salts, described above, the cations and anions in [**C0**][$C(CN)_3$] appear to be independently stacked along the *b*-axis to form a columnar structure. This segregated-stack structure is formed through intermolecular π–π interactions. The interplanar distance between the $C(CN)_3^-$ anions is approximately 3.3–3.4 Å, while the interplanar distance between the Cp and benzene rings of adjacent cations is 3.5 Å.

In the case of ferrocenium salts having cyano-substituted anions, such as tetracyanoquinodimethane (TCNQ), the cyano groups of the anion are often close to the Fe

atom of the cation (Fe···N = 4.1–4.7 Å).[22] Although these distances are larger than the sum of the respective van der Waals radii, such a close arrangement is accompanied by electrostatic interactions.[22] In the case of [**C0**][$C(CN)_3$], four cyano groups are located near the ruthenium atom of one of the crystallographically independent cations (Ru1···N = 3.99–4.60 Å; Fig. 4, dotted lines), and two cyano groups are near the ruthenium atom of the other cation (Ru2···N = 4.50, 4.44 Å). Local electrostatic interactions within these arrangements probably stabilize this segregated-stack structure. Similarly, Ru···NC- interactions are also present in [**C0**][$B(CN)_4$], in which two cyano groups are located in close proximity to the Ru atom (Ru···N = 4.13 Å).

Cations and anions often form alternating arrangements in the crystals of sandwich complex salts. For example, metallocenium salts containing tetracyanoethylene anions exhibit a mixed-stack structure,[23] whereas those with tetracyanoquinodimethane anions exhibit both mixed- and segregated-stack structures.[24] The significantly lower melting points of the $C(CN)_3$ salts, when compared with salts containing other anions, can be ascribed to weaker electrostatic interactions between the cations and anions in these salts, owing to their segregated-stack structures. In the crystals of [FeL_2][$C(CN)_3$] (L = C_5Me_5 or C_6Me_6),[13,14] the cations and anions are alternately arranged, which demonstrates that salts containing $C(CN)_3^-$ can also form mixed-stack structures.

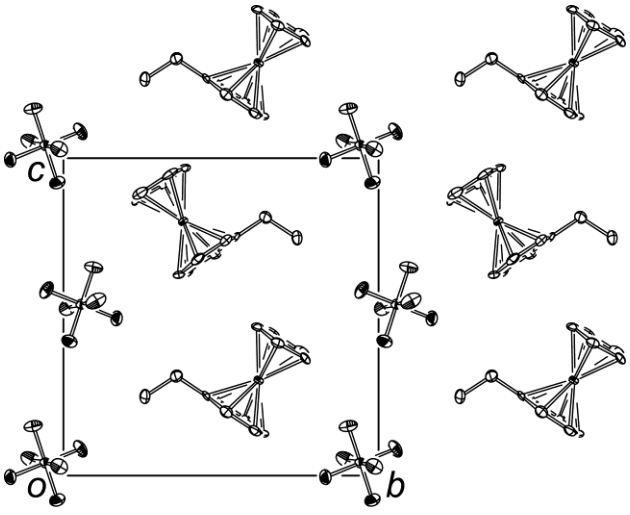

Fig. 3 Packing diagram of [**C2**][PF_6] viewed along the *a*-axis. Hydrogen atoms have been omitted for clarity.

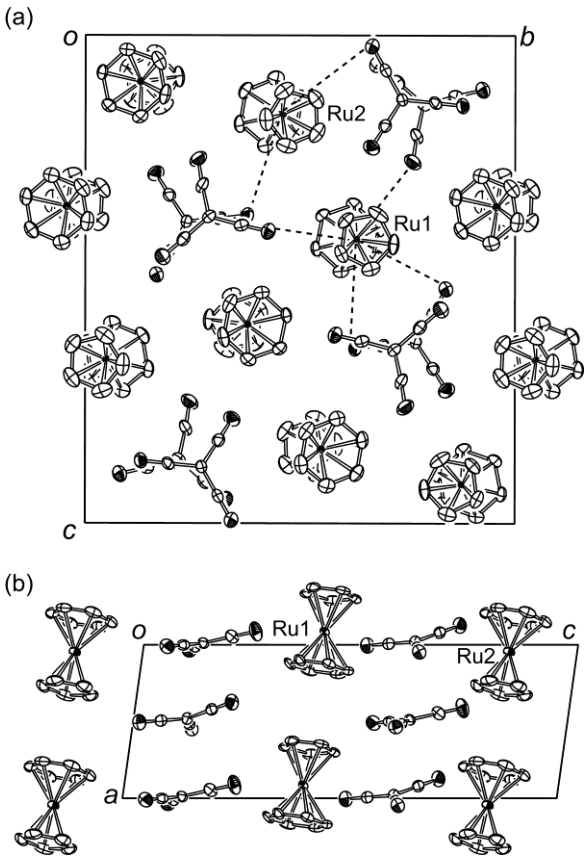

Fig. 4 Packing diagrams of [**C0**][$C(CN)_3$] viewed along (a) the stacking axis, and (b) perpendicular to the stacking axis. Dotted lines represent Ru···NC- close separations. Hydrogen atoms have been omitted for clarity.

Powder X-ray diffraction of plastic crystals

The [**C1**][PF_6] and [**C1**][$B(CN)_4$] salts exhibit plastic phases at room temperature, whereas [**C0**][$B(CN)_4$], [**C1**][FSA] and [**C2**][PF_6] only exhibit plastic phases at high temperatures. From the XRD patterns (Figs. 5 and S9; ESI†), the plastic phases are found to have CsCl-type cubic lattices in common, with lattice constants of 7.136(7)–7.667(16) Å (Table 3). The

interionic distances in these crystals were calculated to be 6.177(6)–6.638(14) Å, which are in excellent agreement with the sum of the ionic radii estimated by DFT calculations (6.27–6.69 Å, Table 3). The radius ratio rule for ionic crystals predicts NaCl-type structures for anion–cation radius ratios of 0.41–0.73, and CsCl-type structures for ratios larger than 0.73.[21] The radius ratios (r_{anion}/r_{cation}) of [**C1**][B(CN)$_4$], [**C0**][B(CN)$_4$] and [**C1**][FSA] lie between 0.78 and 0.86, and are larger than 0.73. Therefore, their CsCl-type structures are in agreement with the rule, although [**C1**][PF$_6$] and [**C2**][PF$_6$], with smaller radius ratios, (0.72 and 0.70, respectively) also exhibit the same structures.

The XRD pattern of [**C1**][FSA] in the room temperature phase (phase II, Fig. 2b), which is below the plastic phase, also exhibits a relatively small number of peaks (Fig. S9b; ESI†). This feature indicates that this phase is highly disordered, accounting for the appearance of this material as a greasy solid at room temperature, and is consistent with its small phase transition entropy to the plastic phase.

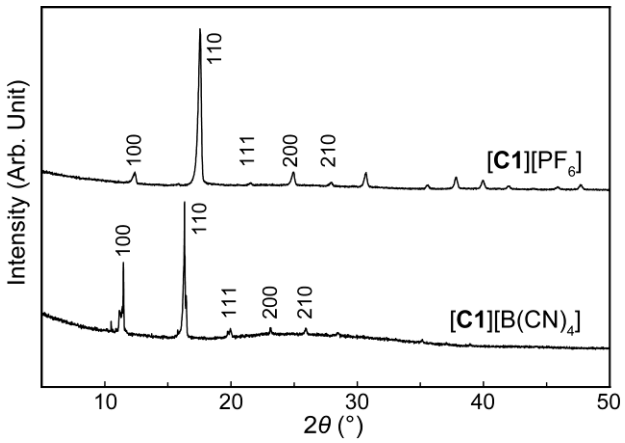

Fig. 5 Powder XRD patterns of [**C1**][PF$_6$] and [**C1**][B(CN)$_4$] at room temperature.

Table 3 Lattice constants (a) and interionic distances (r^{+-}) determined from powder XRD measurements, sum of calculated ionic radii ($r_{cation}+r_{anion}$), and radius ratios (r_{anion}/r_{cation}) of the salts.

	Temperature (°C)	a (Å)	r^{+-} (Å)	$r_{cation}+r_{anion}$ (Å)[a]	r_{anion}/r_{cation} [a]
[**C1**][PF$_6$]	20	7.136(7)	6.177(6)	6.27	0.72

[**C1**][$B(CN)_4$]	20	7.667(16)	6.638(14)	6.69	0.83
[**C0**][$B(CN)_4$]	80	7.50(5)	6.50(4)	6.58	0.86
[**C1**][FSA]	80	7.49 [b]	6.49 [b]	6.52	0.78
[**C2**][PF_6]	100	7.23 [b]	6.26 [b]	6.38	0.70

[a]Calculated values based on DFT calculations (Tables S1 and S2, ESI†). [b]Standard deviations are not given due to instrumental limitation.

Conclusion

This study investigated the phase behavior of the salts of cationic sandwich complexes, focusing on the effect of the substituents on the cation, and the anionic species. Among the salts having non-planar anions, [**C0**][X] and [**C1**][X] were solids that exhibited plastic crystal phases, whereas most of [**C2**][X] and [**C4**][X] exhibited liquid phases at or above room temperature. Unsubstituted salts, or those containing methyl groups, exhibited plastic phases owing to the spherical shape of the cation, whereas salts with longer substituents showed ionic liquid behavior resulting from the lower melting point caused by the conformational freedom of the substituent.

Salts containing the planar anion $C(CN)_3^-$ were exceptional in that they exhibited relatively low melting points regardless of the substituent on the cation. Even the salt lacking an alkyl chain [**C0**][$C(CN)_3$] exhibited a melting point below 100 °C, and this feature is likely to be the result of the formation of a segregated-stack crystal structure, which is accompanied by small cation–anion electrostatic interactions. The planar anion was therefore found to be useful for the synthesis of ionic liquids from sandwich complexes, and this indicates that the control of melting point based on crystal engineering is possible.

This study revealed a molecular design strategy for producing ionic liquids and ionic plastic crystals from sandwich complexes. These results will be useful for the future development of organometallic functional ionic materials.

Experimental

General

[**C0**][PF_6],[8] [**C1**][PF_6],[9] [**C2**][PF_6],[25] and [**C0**][FSA][4d] were synthesized following literature procedures. K[$C(CN)_3$] was used after double recrystallization from ethanol. The van der Waals volumes of cations and anions were estimated based on DFT calculations.[26] The Spartan '14 software (Wavefunction Inc.) was used for the calculations (B3LYP/Lanl2DZ), and the radii of the ions were tentatively calculated assuming spheres having the same volume with the ions. Molecular volumes and radii of cations and anions are listed in Tables S1 and S2 (ESI†). ^{1}H NMR spectra were recorded using a Bruker Avance III 400-MHz spectrometer. Elemental analyses were performed on a PerkinElmer 2400II elemental analyzer. DSC measurements were performed using a TA Q100 differential scanning calorimeter in sealed aluminum pans at a scan rate of 10 K min^{-1} (other rates were applied as required). Powder XRD measurements at room temperature were performed by using a Rigaku SmartLab diffractometer with CuKα radiation (λ = 1.5418 Å). Powder X-ray diffraction data at high temperatures were collected by using a Bruker APEX II Ultra CCD diffractometer with MoKα radiation (λ = 0.71073 Å). Indexing of powder XRD data was performed by using a DICVOL06 software.[27] TG analyses were performed using a Rigaku TG8120 at 10 K min^{-1} under nitrogen. The viscosities of the liquid samples were measured using a Toki Sangyo TV-22L viscometer equipped with a 3 R7.7 cone rotor. The VFT fitting was performed using a non-linear least-square method implemented in the IGOR Pro software program, which is based on the Levenberg–Marquardt algorithm. Polarizing microscope observations were performed using an Olympus BX51 microscope.

Synthesis of [Ru(Cp)(C_6H_6)][X] ([C0][X]; X = $B(CN)_4$, $C(CN)_3$)

[C0][$B(CN)_4$]. A solution of [Ru(Cp)(C_6H_6)][PF_6] (83.6 mg, 0.215 mmol) in a mixture of

methanol (20 mL) and acetonitrile (2 mL) was eluted through an anion exchange column (Dowex 1X8-100, chloride form, eluent: methanol). Evaporation of the solution collected from the column left [Ru(Cp)(C_6H_6)]Cl as a pale yellow oil. An aqueous solution of K[$B(CN)_4$] (114 mg, 0.74 mmol) was added to an aqueous solution of [Ru(Cp)(C_6H_6)]Cl thus obtained and stirred for 1 h. The solution was extracted five times using dichloromethane. The organic layer was concentrated, washed with water, dried over magnesium sulfate, and the solvent was evaporated under reduced pressure. The residue was dissolved in acetone, and the addition of diethyl ether to the solution caused separation of a brown oil. Sonication of the mixture precipitated the desired product as a white powder. The powder was collected by filtration and dried under vacuum to yield a white solid (40.5 mg, 53%). ^{1}H NMR (400 MHz, CD_3CN): δ = 5.33 (s, 5H, Cp-*H*$_5$), 6.09 (s, 6H, Ar-*H*$_6$). Anal. Calcd. for $C_{15}H_{11}BN_4Ru$: C, 50.16; H, 3.09; N, 15.60. Found: C, 50.33; H, 3.00; N, 15.70.

[C0][C(CN)$_3$]. This salt was prepared by anion exchange as described for [**C0**][$B(CN)_4$], using [Ru(Cp)(C_6H_6)][PF_6] (198.5 mg, 0.51 mmol) and K[$C(CN)_3$] (79.3 mg, 0.61 mmol). The crude product was recrystallized from a mixture of acetone and diethyl ether, and dried under vacuum to yield a white solid (69.6 mg, 41%). ^{1}H NMR (400 MHz, $CDCl_3$): δ = 5.52 (s, 5H, Cp-*H*$_5$), 6.30 (s, 6H, Ar-*H*$_6$). Anal. Calcd. for $C_{15}H_{11}N_3Ru$: C, 53.89; H, 3.32; N, 12.57. Found: C, 53.89; H, 3.20; N, 12.59.

Synthesis of [Ru(Cp)($C_6H_5CH_3$)][X] ([C1][X]; X = $B(CN)_4^-$, $C(CN)_3^-$, and FSA^-)

[C1][FSA]. An aqueous solution of K[FSA] (212 mg, 0.966 mmol) was added to a solution containing [Ru(Cp)($C_6H_5CH_3$)][PF_6] (130 mg, 0.323 mmol) in a mixture of water and acetone, and the resulting solution was stirred for 30 min. After acetone evaporation, the resulting suspension was extracted five times using dichloromethane, and the organic layer was washed

once with water. The solution was dried over magnesium sulfate, the solvent was evaporated under reduced pressure, and subsequently passed through a short plug of alumina (eluent: acetonitrile). After evaporation of the solvent under reduced pressure, the residue was dissolved in hot ethanol and cooled slowly to yield the desired product as a white solid (76.7 mg, 54%). ^{1}H NMR (400 MHz, CD_3CN): δ = 2.28 (s, 3H, C*H*$_3$, *J* = 7.6 Hz), 5.27 (s, 5H, Cp-*H*$_5$), 5.96–6.08 (m, 5H, Ar-*H*$_5$). Anal. Calcd. for $C_{12}H_{13}F_2NO_4RuS_2$: C, 32.87; H, 2.99; N, 3.19. Found: C, 33.09; H, 2.95; N, 3.11.

[C1][B(CN)$_4$]. As described for [**C0**][$B(CN)_4$], this salt was prepared by anion exchange, using [Ru(Cp)($C_6H_5CH_3$)][PF_6] (89.5 mg, 0.222 mmol) and K[$C(CN)_3$] (54.0 mg, 0.351 mmol). The crude product was recrystallized from a mixture of acetone and diethyl ether and subsequently dried under vacuum to yield a white solid (62.7 mg, 76%). ^{1}H NMR (400 MHz, CD_3CN): δ = 2.30 (s, 3H, C*H*$_3$), 5.29 (s, 5H, Cp-*H*$_5$), 5.98–6.10 (m, 5H, Ar-*H*$_5$). Anal. Calcd. for $C_{16}H_{13}BN_4Ru$: C, 51.50; H, 3.51; N, 15.01. Found: C, 51.62; H, 3.34; N, 15.04.

[C1][C(CN)$_3$]. As described for [**C0**][$B(CN)_4$], this salt was prepared by anion exchange using [Ru(Cp)($C_6H_5CH_3$)][PF_6] (200 mg, 0.50 mmol) and K[$C(CN)_3$] (83.8 mg, 0.65 mmol). The crude product was purified by column chromatography (activated alumina, eluent: chloroform followed by acetonitrile, R_f = 0.2). The solvent was evaporated from the eluent under reduced pressure after which the desired product was obtained as a pale yellow liquid (94.6 mg, 73%). The liquid was further dried overnight under vacuum at room temperature. ^{1}H NMR (400 MHz, CD_3CN): δ = 2.08 (s, 3H, C*H*$_3$), 5.07 (s, 5H, Cp-*H*$_5$), 5.75–5.88 (m, 5H, Ar-*H*$_5$). Anal. Calcd. for $C_{15}H_{13}N_3Ru$: C, 55.16; H, 3.76; N, 12.06. Found: C, 54.91. H, 3.78. N, 12.28. The liquid was unstable against heat, turning to brown at 50 °C within a few hours.

Synthesis of [Ru(Cp)($C_6H_5CH_3$)][X] ([C2][X]; X = $B(CN)_4^-$, $C(CN)_3^-$, and FSA^-)

[C2][FSA]. As described for [**C1**][FSA], this salt was prepared by anion exchange using [Ru(Cp)($C_6H_5C_2H_5$)][PF_6] (140 mg, 0.335 mmol) and K[FSA] (218 mg, 0.994 mmol), except that after passing the crude product through the short plug of alumina, the product was obtained by evaporation of the solvent under reduced pressure. A pale yellow liquid was obtained (54.4 mg, 36%), which was further dried overnight under vacuum at 90 °C. ^{1}H NMR (400 MHz, CD_3CN): δ = 1.20 (t, 3H, C*H*$_3$, *J* = 7.6 Hz), 2.53 (q, 2H, C*H*$_2$, *J* = 7.52 Hz), 5.30 (s, 5H, Cp-*H*$_5$), 6.00–6.09 (m, 5H, Ar-*H*$_5$). Anal. Calcd. for $C_{13}H_{15}F_2NO_4RuS_2$: C, 34.51; H, 3.34; N, 3.10. Found: C, 34.89; H, 3.74; N, 3.32.

[C2][B(CN)$_4$]. As described for [**C0**][$B(CN)_4$], [Ru(Cp)($C_6H_5C_2H_5$)]Cl was prepared by anion exchange using [Ru(Cp)($C_6H_5C_2H_5$)][PF_6] (210 mg, 0.503 mmol). An aqueous solution of K[$B(CN)_4$] (114 mg, 0.74 mmol) was added to an aqueous solution of the as-obtained [Ru(Cp)(C_6H_6)]Cl and stirred for 30 min. The resulting solution was extracted five times using dichloromethane. The organic layer was washed once with water, dried over magnesium sulfate, and the solvent was evaporated under reduced pressure. The resulting pale yellow residue was dissolved in acetonitrile and passed through a short plug of alumina (eluent: acetonitrile). The solvent was evaporated under vacuum to yield a pale yellow liquid (139 mg, 72%), which was further dried overnight at 70 °C under vacuum. ^{1}H NMR (400 MHz, CD_3CN): δ = 1.21 (t, 3H, C*H*$_3$, *J* = 7.52 Hz), 2.53 (q, 2H, C*H*$_2$, *J* = 7.52 Hz), 5.30 (s, 5H, Cp-*H*$_5$), 6.02–6.09 (m, 5H, Ar-*H*$_5$). Anal. Calcd. for $C_{17}H_{15}BN_4Ru$: C, 52.73; H, 3.90; N, 14.47. Found: C, 52.57; H, 4.03; N, 14.54.

[C2][C(CN)$_3$]. As described for [**C2**][$B(CN)_4$], this salt was prepared by anion exchange using [Ru(Cp)($C_6H_5C_2H_5$)][PF_6] (187 mg, 0.448 mmol) and K[$C(CN)_3$] (86.7 mg, 0.672

mmol). The product was obtained as a pale yellow liquid (103 mg, 64%), which was dried overnight under vacuum at room temperature. ^{1}H NMR (400 MHz, CD_3CN): δ = 1.21 (t, 3H, C*H*$_3$, *J* = 7.56 Hz), 2.05 (q, 2H, C*H*$_2$, *J* = 7.60 Hz), 5.30 (s, 5H, Cp-*H*$_5$), 6.00–6.10 (m, 5H, Ar-*H*$_5$). Anal. Calcd. for $C_{17}H_{13}N_4Ru$: C, 56.34; H, 4.17; N, 11.60. Found: C, 56.12; H, 3.96; N, 11.54.

Synthesis of [Ru(Cp)($C_6H_5C_4H_9$)][X] ([C4][X]; X = $B(CN)_4^-$ and $C(CN)_3^-$)

[C4][B(CN)$_4$]. As described for [**C2**][$B(CN)_4$], this salt was prepared by anion exchange using [Ru(Cp)($C_6H_5C_4H_9$)][FSA] (162.6 mg, 0.34 mmol) and K[$B(CN)_4$] (115.0 mg, 0.77 mmol). The product was obtained as a pale yellow liquid (72.0 mg, 64%), which was dried overnight at 70 °C under vacuum. ^{1}H NMR (400 MHz, CD_3CN): δ = 0.94 (t, 3H, C*H*$_3$, *J* = 7.30 Hz), 1.36–1.42 (m, 2H, C*H*$_2$), 1.52–1.60 (m, 2H, C*H*$_2$), 2.50–2.46 (m, 2H, C*H*$_2$), 5.29 (s, 5H, Cp-*H*$_5$), 5.98–6.08 (m, 5H, Ar-*H*$_5$). Anal. Calcd. for $C_{19}H_{19}N_4BRu$: C, 54.95; H, 4.61; N, 13.49. Found: C, 54.97; H, 4.76; N, 13.49.

[C4][C(CN)$_3$]. As described for [**C2**][$B(CN)_4$], this salt was prepared by anion exchange using [Ru(Cp)($C_6H_5C_4H_9$)][PF_6] (130.0 mg, 0.229 mmol) and K[$C(CN)_3$] (56.5 mg, 0.438 mmol). The product was obtained as a pale yellow liquid (118.7 mg, 84%), which was dried overnight at room temperature under vacuum. ^{1}H NMR (400 MHz, CD_3CN): δ = 0.94 (t, 3H, C*H*$_3$, *J* = 7.33 Hz), 1.34–1.43 (m, 2H, C*H*$_2$), 1.51–1.59 (m, 2H, C*H*$_2$), 2.48–2.48 (m, 2H, C*H*$_2$), 5.29 (s, 5H, Cp-*H*$_5$), 5.99–6.08 (m, 5H, Ar-*H*$_5$). Anal. Calcd. for $C_{19}H_{19}N_3Ru$: C, 58.45; H, 4.90; N, 10.76. Found: C, 58.06; H, 4.16; N, 10.70.

X-ray crystallography

Single crystals of [**C0**][$C(CN)_3$] and [**C2**][PF_6], grown by recrystallization from a mixture of

acetone and diethyl ether, were used for single crystal X-ray crystallography. XRD data were collected by using a Bruker APEX II Ultra CCD diffractometer with MoKα radiation (λ = 0.71073 Å). All calculations were performed using SHELXTL.[28] ORTEP-3 for Windows was used to generate the molecular graphics.[29] ORTEP drawings of the molecular structures are shown in Fig. S10 (ESI†). The crystallographic parameters are listed in Table 4.

We also performed structure determination of [**C0**][FSA] and [**C0**][$B(CN)_4$] at 296 and 173 K, respectively. However, refinements were unsatisfactory because of extensive disorder. Therefore, we refrained from detailed discussion. Although the space group of [**C0**][FSA] was considered to be *C*2/m, the refinements were tentatively performed by assuming a space group *C*2 because the Cp and benzene rings are overlapped by disorder, thereby making their refinements impossible in the higher symmetry space group. For the same reason, the structure of [**C0**][$B(CN)_4$] was tentatively refined in group *A*ma2 although the actual space group was considered to be *C*mc2_1. The tentative *R* values for the structures were R_1 = 0.039 and wR_2 = 0.114 for [**C0**][$B(CN)_4$] and R_1 = 0.037 and wR_2 = 0.099 for [**C0**][FSA]. Their cell parameters and packing diagrams are shown in the Supporting Information (Table S4 and Fig. S8; ESI†).

Table 4 Crystallographic parameters

	[**C0**][$C(CN)_3$]	[**C2**][PF_6]
Empirical formula	$C_{15}H_{11}N_3Ru$	$C_{13}H_{15}F_6PRu$
Formula weight	334.34	417.29
Crystal system	Monoclinic	Orthorhombic
Space group	$P2_1/n$	$P2_12_12_1$
a (Å)	7.2376(14)	8.7719(17)
b (Å)	17.759(3)	12.685(2)
c (Å)	20.303(4)	12.779(3)
β (°)	97.971(2)	90
V (Å^3)	2584.5(9)	1421.9(5)
Z	8	4

$d_{calcd.}$ (mg m^{-3})	1.719	1.949
T (K)	173	100
μ (mm^{-1})	1.200	1.271
Reflections collected	13058	7574
Independent reflections	4896 (R_{int} = 0.0649)	2991 (R_{int} = 0.0802)
F(000)	1328	824
$R_1{}^a$, $wR_2{}^b$ ($I > 2\sigma$(I))	0.0373, 0.0873	0.0469, 0.1128
$R_1{}^a$, $wR_2{}^b$ (all data)	0.0449, 0.0929	0.0480, 0.1140
Goodness-of-fit on F^2	1.038	1.045
Completeness to θ (%)	99.9	99.7
Parameters	343	191
Largest diff. peak and hole	0.906 and –0.617	1.297 and –2.423

$^aR_1 = \Sigma\ ||F_o| - |F_c|| / \Sigma\ |F_o|$. $^bwR_2 = [\ \Sigma\ w(F_o^2 - F_c^2)^2 / \Sigma\ w(F_o^2)^2]^{1/2}$.

Acknowledgments

This work was financially supported by KAKENHI (grant number 16H04132) from the Japan Society for the Promotion of Science (JSPS). We are grateful to Dr. Y. Funasako (Tokyo University of Science, Yamaguchi) for discussion.

References

1. A. Stark and K. R. Seddon, in *Kirk-Othmer Encyclopedia of Chemical Technology*, Wiley-Interscience, New York, 5th edn, **2007**, vol. *26*, pp. 836–919.

2. a) Y. Yoshida and G. Saito, in Ionic Liquids: Theory, Properties, New Approaches, ed. A. Kokorin, InTech, 2011, chap. 29, pp. 723–738; b) R. E. Del Sesto, C. Corley, A. Robertson and J. Wilkes, *J. Organomet. Chem.*, 2005, **690**, 2536–2542; c) A. Branco, L. C. Branco and F. Pina, *Chem. Commun*., 2011, **47**, 2300–2302; d) P. Zhang, Y. Gong, Y. Lv, Y. Guo, Y. Wang, C. Wang and H. Li, *Chem. Commun*., 2012, **48**, 2334–2336; e) P. Nockemann, B. Thijs, N. Postelmans, K. Van Hecke, L. Van Meervelt and K. Binnemans, *J. Am. Chem. Soc*., 2006, **128**, 13658–13659; f) B. Mallick, B. Balke, C. Felser and A.-V. Mudring, *Angew. Chem., Int. Ed*., 2008, **47**, 7635–7638; g) R. J. C. Brown, P. J. Dyson, D. J. Ellis and T. Welton, *Chem. Commun*., 2001, **3**, 1862–1863; h) M. Okuhata, Y. Funasako, K. Takahashi and T. Mochida, *Chem. Commun*., 2013, **49**, 7662–7664.

3. a) H. Masui and R. W. Murray, *Inorg. Chem.*, 1997, **36**, 5118–5126; b) I. J. B. Lin and C. S.

Vasam, *J. Organomet. Chem*., 2005, **690**, 3498–3512; c) J. F. Huang, H. M. Luo and S. Dai, J. *Electrochem. Soc*., 2006, **153**, J9–J13; d) M. Iida, C. Baba, M. Inoue, H. Yoshida, E. Taguchi and H. Furusho, *Chem. Eur. J*., 2008, **14**, 5047–5056; e) H. D. Pratt III, A. J. Rose, C. L. Staiger, D. Ingersoll and T. M. Anderson, *Dalton Trans*., 2011, **40**, 11396–11401; f) N. R. Brooks, S. Schaltin, K. Van Hecke, L. Van Meervelt, K. Binnemans and J. Fransaer, *Chem. Eur. J*., 2011, **17**, 5054–5059; g) Y. Funasako, T. Mochida, K. Takahashi, T. Sakurai and H. Ohta, *Chem. Eur. J*., 2012, **18**, 11929–11936; h) M. Okuhata, Y. Funasako, K. Takahashi and T. Mochida, *Chem. Commun*., 2013, **49**, 7662–7664; i) Y. Funasako, M. Nosho and T. Mochida, *Dalton Trans*., 2013, **42**, 10138–10143; j) Y. Miura, F. Shimizu and T. Mochida, *Inorg. Chem*., 2010, **49**, 10032–10040.

4. a) T. Inagaki, T. Mochida, M. Takahashi, C. Kanadani, T. Saito and D. Kuwahara, *Chem. Eur. J.* 2012, **18**, 6795–6804; b) T. Inagaki, T. Mochida, *Chem. Lett*. 2010, **39,** 572–573; c) Y. Funasako, T. Inagaki, T. Mochida, T. Sakurai, H. Ohta, K. Furukawa and T. Nakamura, *Dalton Trans*. 2013, **42**, 8317–8327; d) Y. Funasako, S. Mori and T. Mochida, *Chem. Commun*., 2016, **52**, 6277–6279.

5. a) D. Braga and F. Grepioni, *Chem. Soc. Rev*. 2000, **29,** 229–238; b) D. Braga and F. Grepioni, in *Topics in Organometallic Chemistry* (Eds.: J. M. Brown, P. Hofmann), Springer, Berlin, Heidelberg, 1999, pp. 47–68; c) D. Braga, M. Curzi, S. L. Giaffreda, F. Grepioni, L. Maini, A. Pettersen and M. Polito, in *Ferrocenes: Ligands, Materials and Biomolecules*, (Ed.: P. Štěpnička), Wiley, Chichester, 2008, Chapter 12; d) R. J. Webb, M. D. Lowery, Y. Shiomi, M. Sorai, R. J. Wittebort and D. N. Hendrickson, *Inorg. Chem.* 1992, **31**, 5211–5219; e) F. Grepioni, G. Cojazzi, S. M. Draper, N. Scully and D. Braga, *Organometallics*, 1998, **17,** 296–307; f) H. Schottenberger, K. Wurst, U. J. Griesser, R. K. R. Jetti, G. Laus, R. H. Herber, I. Nowik, *J. Am. Chem. Soc*., 2005, **127**, 6795–6801; g) L. Nowik, R. H. Herber, *Inorg. Chem. Acta* 2000, **310**, 191–195; h) T. Mochida, Y. Funasako, T. Inagaki, M. -J. Li, K. Asahara and D. Kuwahara, *Chem. Eur. J*., 2013, **19**, 6257–6264; i) T. Mochida, Y. Funasako, M. Ishida, S. Saruta, T. Kosone and T. Kitazawa, *Chem. Eur. J.*, 2016, **22**, 15725–15732.

6. a) D. R. MacFarlane, J. Huang and M. Forsyth, *Nature*, 1999, **402**, 792–794; b) J. M. Pringle, *Phys. Chem. Chem. Phys*., 2013, **15,** 1339–1351; c) K. Matsumoto, U. Harinaga, R. Tanaka, A. Koyama, R. Hagiwara and K. Tsunashima, *Phys. Chem. Chem. Phys*., 2014, **16**, 23616–23626; d) Y. Abu-Lebdeh, P. J. Alarco and M. Armand, *Angew. Chem. Int. Ed*., 2003, **42**, 4499–4501; e) Z. B. Zhou and H. Matsumoto, *Electrochem. Commun*., 2007, **9,** 1017–1022; f) J. Luo, A. H. Jensen, N. R. Brooks, J. Sniekers, M. Knipper, D. Aili, Q. Li, B. Vanroy,

M. Wübbenhorst, F. Yan, L. V. Meervelt, Z. Shao, J. Fang, Z. H. Luo, D. E. De Vos, K. Binnemans and J. Fransaer, *Energy Environ. Sci*., 2015, **8**, 1276–1291; g) M. Lee, U. H. Choi, S. Wi, C. Slebodnick, R. H. Colby and H. W. Gibson, *J. Mater. Chem.*, 2011, **21**, 12280–12287.

7. a) A. Komurasaki, Y. Funasako and T. Mochida, *Dalton Trans.*, 2015, **44**, 7595–7605; b) T. Higashi, T. Ueda and T. Mochida, *Phys. Chem. Chem. Phys.*, 2016, **18**, 10041–10048.

8. F. Grepioni, G. Cojazzi, D. Braga, E. Marseglia, L. Scaccianoce and B. F. G. Johnson, *J. Chem. Soc., Dalton Trans.*, 1999, 553–558.

9. A. M. Mcnair, J. L. Schrenk and K. R. Mann, *Inorg. Chem.*, 1984, **23**, 2633–2640.

10. a) D. Turnbull and M. H. Cohen, Modern Aspect of the Vitreous State, Butterworth, London, 1960, vol. 1, p. 38; b) O. Yamamuro, Y. Minamimoto, Y. Inamura, S. Hayashi and H. Hamaguchi, *Chem. Phys. Lett*., 2006, **423**, 371–375.

11. T. Inagaki, T. Mochida, M. Takahashi, C. Kanadani, T. Saito and D. Kuwahara, *Chem. Eur. J.*, 2012, **18**, 6795–6804.

12. J. Luo, O. Conrad and I. F. J. Vankelecom, *J. Mater. Chem. A*, 2013, **1**, 2238–2247.

13. D. A. Dixon, J. C. Calabrese and J. S. Miller, *J. Am. Chem. Soc.*, 1986, **108**, 2582–2588.

14. J. K. Kochi and C. H. Wei, *J. Organomet. Chem.*, 1993, **451**, 111–121.

15. a) M. Marszalek, Z. Fei, D. Zhu, R. Scopelliti, P. J. Dyson, S. M. Zakeeruddin and M. Grätzel, *Inorg. Chem.*, 2011, **50**, 11561–11567; b) G. P. Pandey and S. A. Hashmi, *Bull. Mater. Sci.*, 2013, **36**, 729–733; c) P. Barthen, W. Frank and N. Ignatiev, *Ionics*, 2015, **21**, 149–159.

16. N. V. Ignat'ev, M. Finze, J. A. P. Sprenger, C. Kerpen, E, Bernhardt and H. Willner, *J. Fluorine Chem.*, 2015, **177**, 46–54.

17. Y. Wang, K. Zaghib, A. Guerfi, Fernanda F.C. B, Roberto M. Torresi and J. R. Dahn. *Electrochim. Acta*, 2007, **52**, 6346–6352.

18. a) G. S. Fulcher, *J. Am. Ceram. Soc*., 1925, **8**, 339–355; b) W. Xu, E. I. Cooper and C. A. Angell, *J. Phys. Chem. B*, 2003, **107**, 6170–6178.

19. a) A. Paul and A. J. Samanta, *J. Phys. Chem. B*, 2008, **112**, 16626–16632; b) H. Tokuda, K. Ishii, M. A. B. H. Susan, S. Tsuzuki, K. Hayamizu and M. Watanabe, *J. Phys. Chem. B*, 2006, **110**, 2833–2839.

20. T. Mochida, Y. Funasako, T. Inagaki, M. J. Li, K. Asahara and D. Kuwahara, *Chem. Eur. J.*, 2013, **19**, 6257–6264.

21. P. Atkins, T. Overton, J. Rourke, M. Weller and F. Armstrong, Shriver & Atkins' Inorganic Chemistry, Oxford University Press, Oxford, 2010.

22. T. Mochida, Y. Funasako, E. Nagabuchi and H. Mori, *Cryst. Growth Des.*, 2014, **14**, 1459–1466.

23. J. Her, P. W. Stephenes, J. Ribas-Ariño, J. J. Novoa, W. W. Shum and J. S. Miller, *Inorg. Chem*., 2009, **48**, 3296–3307.

24. a) T. Mochida, T. Akasaka, Y. Funasako, Y. Nishio and H. Mori, *Cryst. Growth Des*., 2013, **13**, 4460–4468; b) Y. Funasako, T. Mochida, T. Sakurai, H. Ohta, T. Akasaka and Y. Nishio, *Inorg. Chim. Acta*., 2014, **419**, 105−110.

25. N. A. Vol'kenau, I. N. Bolesova, L. S. Shul'pina, A. N. Kitaigorodskii and D. N. Kravtsov, *J. Organomet. Chem.*, 1985, **288**, 341–348.

26. N. Terasawa, I. Takeuchi, H. Matsumoto, *Sens. Actuators B,* 2009, **139**, 624–630.

27. A. Boultif and D. Louër, *J. Appl. Cryst.*, 2004, **37**, 724–731.

28. G. M. Sheldrick, *Acta Crystallogr*. 2008, **A64**, 112−122.

29. L. J. Farrugia, *J. Appl. Crystallogr*. 1999, **32**, 837−838.

TOC

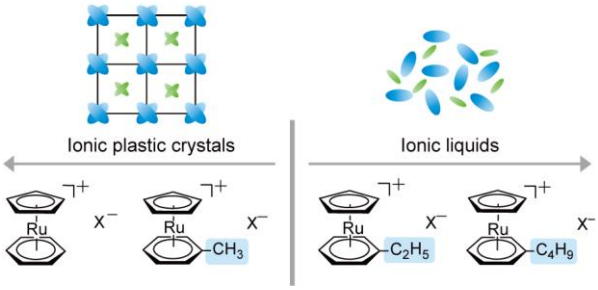

Salts of cationic ruthenium sandwich complexes bearing ethyl or longer substituents are ionic liquids, whereas salts with shorter substituents showed ionic plastic crystal phases.

Supporting Information

Effects of Substituents and Anions on the Phase Behavior of Ru(II) Sandwich Complexes: Exploring the Boundaries between Ionic Liquids and Ionic Plastic Crystals

Takumi Tominaga, Takahiro Ueda, Tomoyuki Mochida*

Department of Chemistry, Graduate School of Science, Kobe University, Kobe, Hyogo 657-8501, Japan. E-mail: tmochida@platinum.kobe-u.ac.jp

Table S1 Volumes and radii of anions estimated by DFT calculations.

anion	V (Å^3)	r_{anion} (Å)
PF_6^-	74.9	2.61
$C(CN)_3^-$	90.8	2.79
FSA^-	98.7	2.87
$B(CN)_4^-$	117.2	3.04
Tf_2N^-	157.5	3.35

Table S2 Volumes and radii of cations estimated by DFT calculations.

cation	V (Å^3)	r_{cation} (Å)
[**C0**]$^+$	186.6	3.54
[**C1**]$^+$	204.9	3.66
[**C2**]$^+$	223.1	3.76
[**C4**]$^+$	260.0	3.96

Table S3 Phase transition data of the salts investigated herein.[a]

	Phase transition	T_c (°C)	ΔH (kJ mol^{-1})	ΔS (J mol^{-1} K^{-1})
[**C0**][PF_6] [b]	I → II	59.3	4.16	12.5
[**C0**][FSA]	I → II	159.8	9.7	22.2
	II → III*	182.7	6.5	14.2
[**C0**][$B(CN)_4$]	I → II	55.8	7.6	22.9
	II → III*	67.1	8.8	25.6
[**C0**][$C(CN)_3$]	I → II	48.9	10.2	31.6
	II → liq.	90.2	10.1	27.5
[**C1**][PF_6]	I → II*	14.8	8.6	29.0
[**C1**][FSA]	I → II	–8.6	7.7	28.6
	II → III*	45.7	2.5	7.6
[**C1**][$B(CN)_4$]	I → II*	14.2	26.5	91.2
[**C1**][$C(CN)_3$]	liq. → I	–58.6	10.0	45.4
	I → II	–29.7	0.9	3.6
	II → liq.	–1.3	20.4 [d]	73.7 [d]
[**C2**][PF_6]	I → II*	88.3	10.3	28.1
	II* → liq.	161.3	5.8	13.2
[**C2**][FSA]	I → liq.	16.9	18.9	64.6
[**C2**][$B(CN)_4$]	I → II*	15.7		
	II* → liq.	22.6	15.2 [e]	52.2 [e]
[**C4**][PF_6] [c]	I → II	62.8	8.7	26.3
	II → III	73.0	5.6	16.6
	III → liq.	87.0	7.8	22.8

[a]Asterisk symbols (*) denote plastic phases. [b]Data from Ref 8. [c]Data from Ref 7. [d]Including the contribution of a solid phase transition near the melting point that appeared as a shoulder. [e]Including the contribution of the solid phase transition from I to II*.

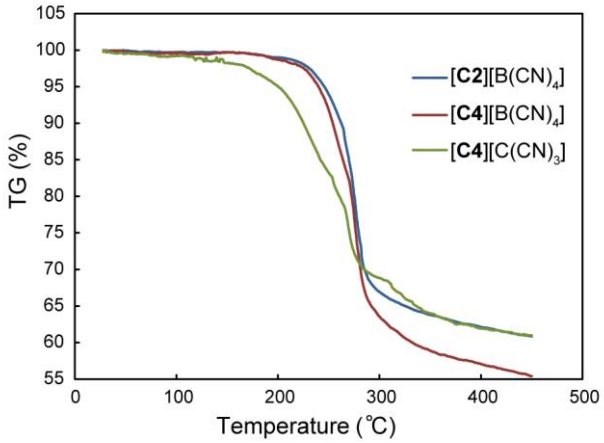

Fig. S1 Thermogravimetric traces of (a) [**C2**][$B(CN)_4$], (b) [**C4**][$B(CN)_4$], and (c) [**C4**][$C(CN)_3$] (10 K min^{-1}).

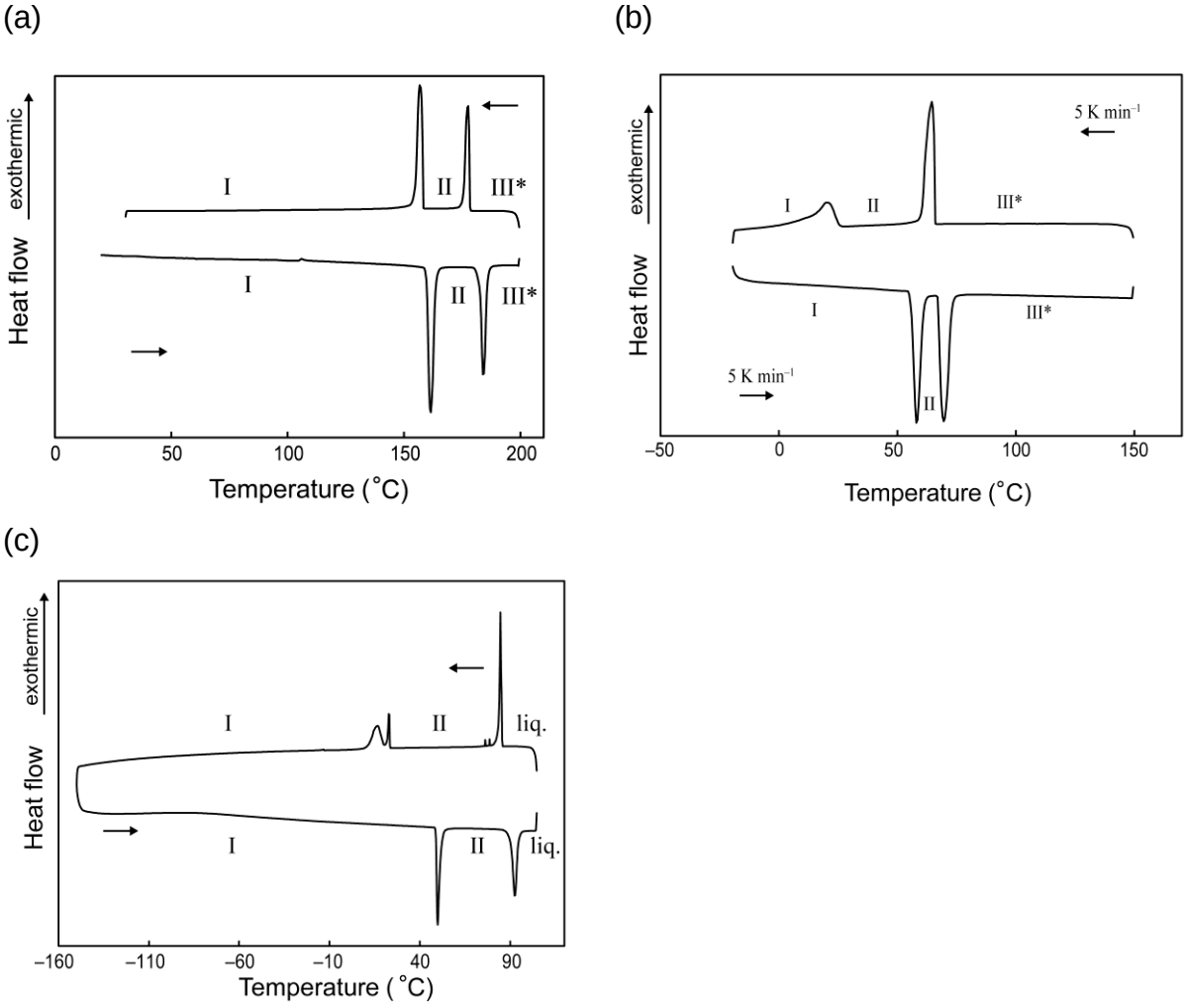

Fig. S2 DSC traces of (a) [**C0**][FSA], (b) [**C0**][$B(CN)_4$], and (c) [**C0**][$C(CN)_3$] (*liq.*: liquid phase). Asterisk symbols (*) denote plastic phases.

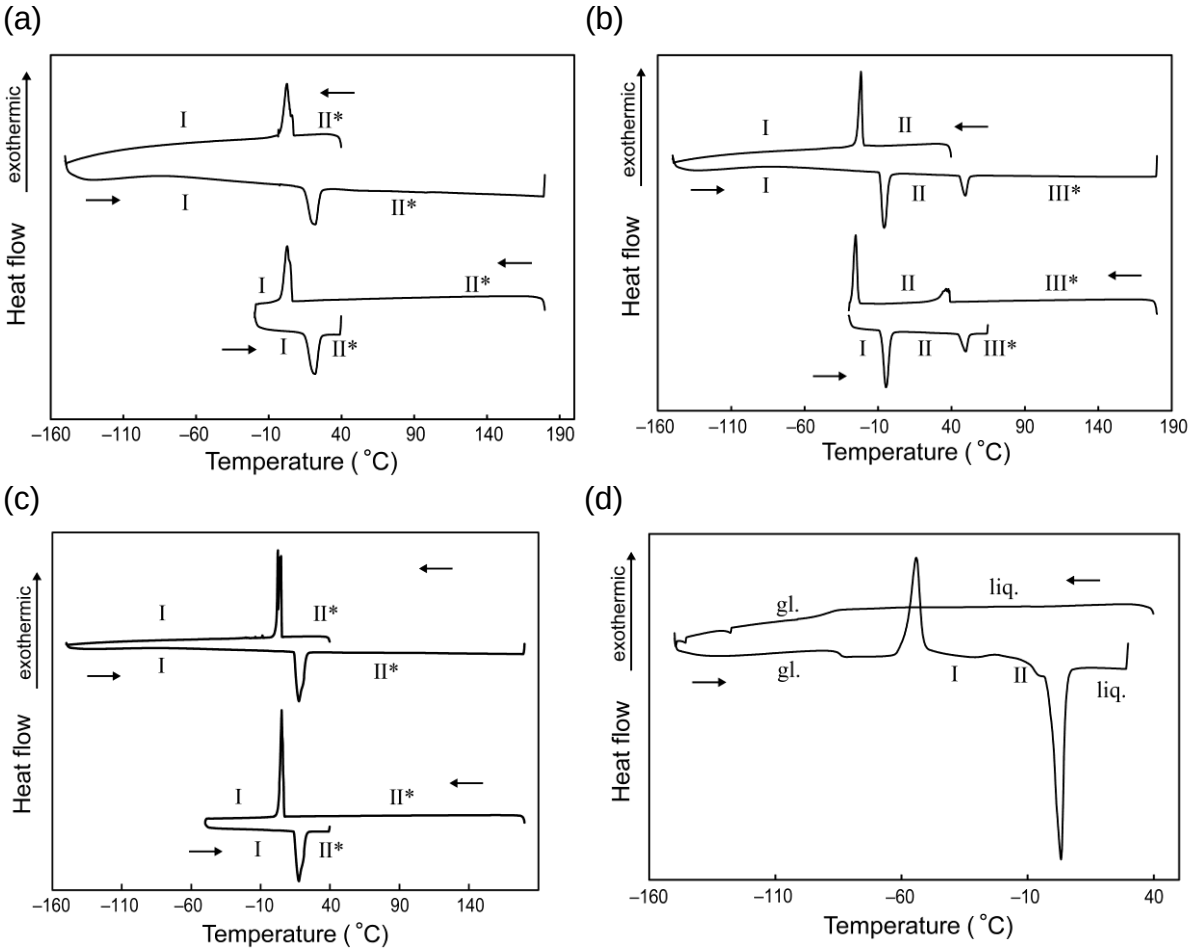

Fig. S3 DSC traces of (a) [**C1**][PF_6], (b) [**C1**][FSA], (c) [**C1**][$B(CN)_4$], and (d) [**C1**][$C(CN)_3$] (*gl.*: glassy phase, *liq.*: liquid phase). Asterisk symbols (*) denote plastic phases.

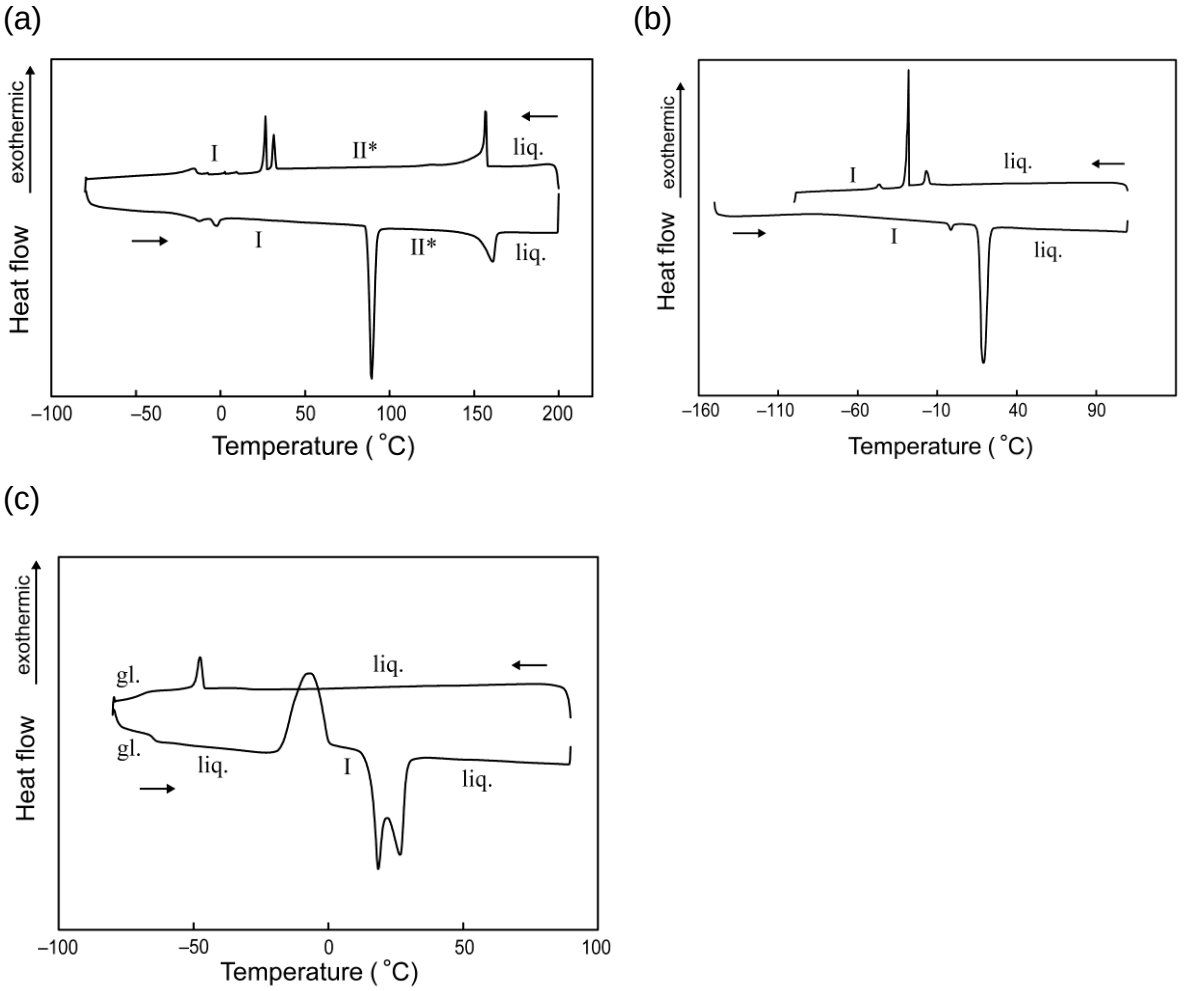

Fig. S4 DSC traces of (a) [**C2**][PF_6], (b) [**C2**][FSA], and (c) [**C2**][$B(CN)_4$] (*gl.*: glassy phase, *liq.*: liquid phase).

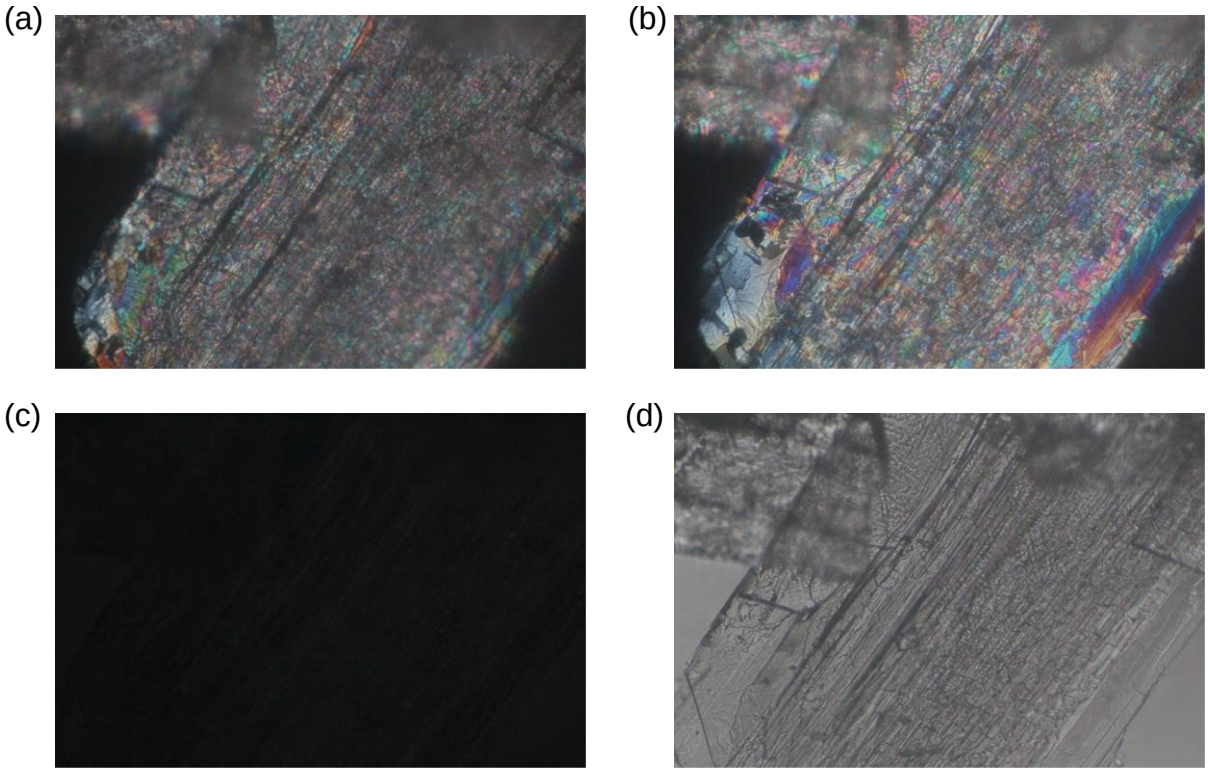

Fig. S5 Polarizing microscope images of [**C0**][FSA] at (a) 25 °C, (b) 170 °C, (c) 200 °C (crossed nicols), and (d) 200 °C (open nicol).

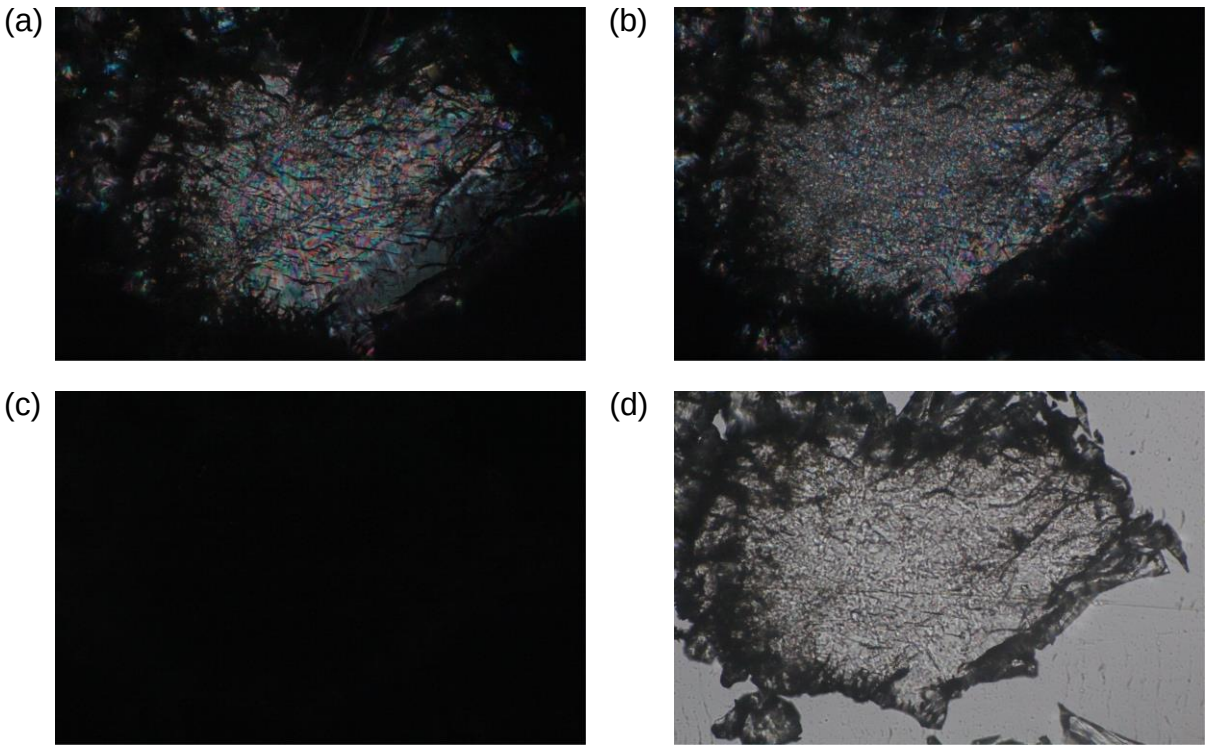

Fig. S6 Polarizing microscope images of [**C0**][$B(CN)_4$] at (a) 25 °C, (b) 60 °C, (c) 80 °C (crossed nicols), and (d) 80 °C (open nicol).

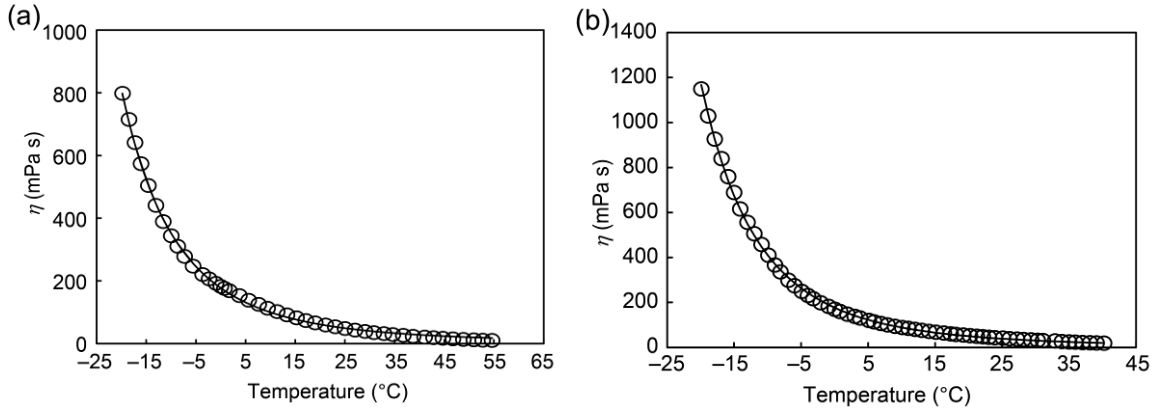

Fig. S7 Temperature dependence of the viscosities of (a) [**C2**][$B(CN)_4$] and (b) [**C4**][$B(CN)_4$]. Solid lines are fitted from the VFT equation.

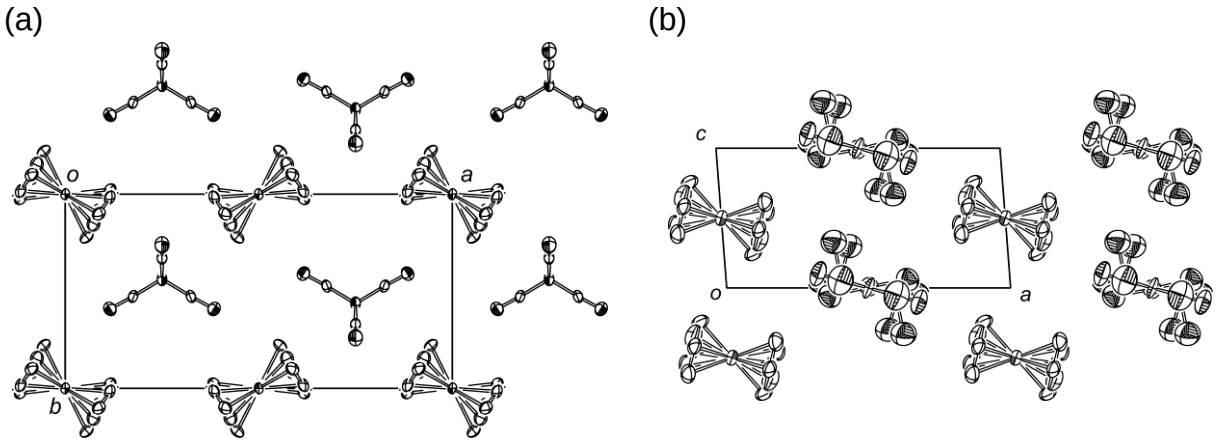

Fig. S8 Packing diagrams of (a) [**C0**][FSA] (296 K) and (b) [**C0**][$B(CN)_4$] (173 K). Hydrogen atoms have been omitted for clarity. Refinements were performed by tentatively assuming the space groups to be *A*ma2 and *C*2, respectively (See text).

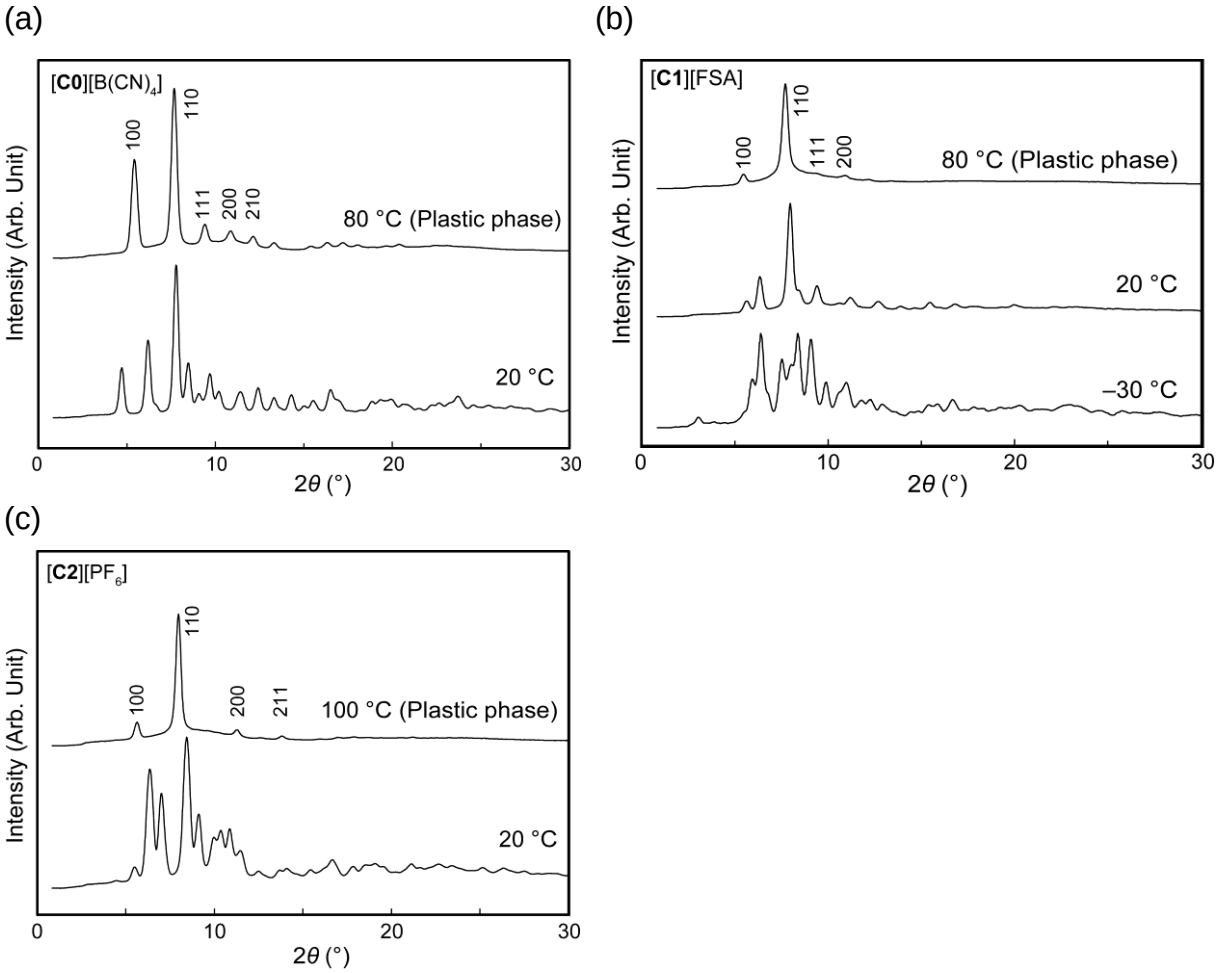

Fig. S9 Powder XRD patterns of (a) [**C0**][$B(CN)_4$], (b) [**C1**][FSA] and (c) [**C2**][PF_6] (MoKα radiation, λ = 0.71073 Å).

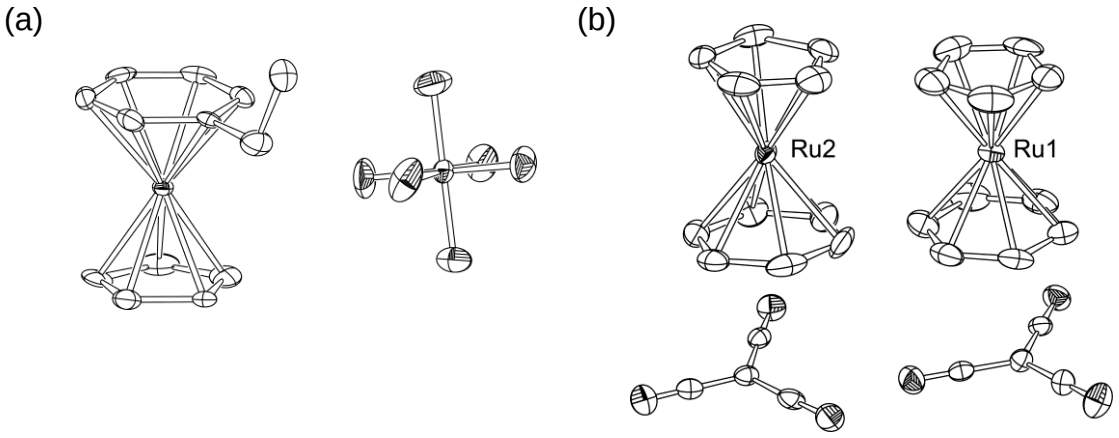

Fig. S10 ORTEP drawings of the molecular structures of (a) [**C2**][PF_6] and (b) [**C0**][$C(CN)_3$]. Hydrogen atoms have been omitted for clarity.

Table S4 Cell parameters of [**C0**][FSA] and [**C0**][$B(CN)_4$]

	[**C0**][FSA]	[**C0**][$B(CN)_4$]
Empirical formula	$C_{11}H_{11}F_2NO_4RuS$	$C_{15}H_{11}N_4BRu$
Formula weight	424.40	359.16
Crystal system	Monoclinic	Orthorhombic
a (Å)	12.856(6)	17.530(10)
b (Å)	8.925(4)	8.791(5)
c (Å)	6.333(3)	9.499(6)
α (°)	69.578(5)	90
β (°)	86.466(6)	90
γ (°)	86.334(5)	90
V (Å^3)	724.5(6)	1463.9(15)
Z	2	4
$d_{calcd.}$ (mg m^{-3})	1.945	1.630
T (K)	296	173